requirements, a huge effort was made to decompose the different shapes/parts into subdomains (Figure 3a). After the optimization, the geometry could be represented by about 15.8 million elements.

Example

Figure 4 shows a zero-offset section from the laboratory data (along the red line denoted in Figure 3b) with interpretation. It is important to highlight here that due to the broad radiation pattern, the laboratory section contains some reflections from the truncated dome (annotated by (c) in Figure 1), which was not included in the numerical simulations.

Figure 4 *Zero-offset cross-section from the laboratory data with interpretation along the red line in Figure 3b. The vertical yellow line corresponds to the yellow asterisk in Figure 3b. Interpreted events: (a) reflection from the top & bottom of the PVC (related to the plateau), (b) reflection from the top & bottom of the PVC (related to the pyramid & dome), (c) reflection from the truncated dome, (d) reflection from the ramp.*

Figure 5 shows an example for the comparison of a laboratory trace with the corresponding synthetic trace, obtained with FEM. The trace is located between the dome and the truncated pyramid, annotated by (a) and (b) in Figure 1, respectively. Furthermore, the trace is denoted by the yellow asterisk in Figure 3b) and the vertical yellow line in Figure 4. Using the annotations in Figure 5, the following interpretation can be given: (a) reflection from the side of the dome, (b) reflection from the side of the pyramid, (c) reflection from the top of the pyramid, (d) diffraction from the edge of the pyramid & diffraction from the edge of the dome, (e) reflection from the bottom of the PVC model below the pyramid, (f) reflection from the bottom of the PVC below the dome & diffraction from the edge of the pyramid.

Comparison between the laboratory (blue) and the synthetic (red) traces shows a very good fit in terms of arrival time and amplitude. However there are some small discrepancies, e.g. in the transition between event (e) and (f). Another small phase-mismatch can be found in case of event (d), or between event (a) and (b). There are two possible reasons for these misfits: 1) the laboratory data is contaminated with noise and 2) the inversion process for the source may not be perfect, also partly due to the noise recorded during the laboratory characterization of the source transducer.

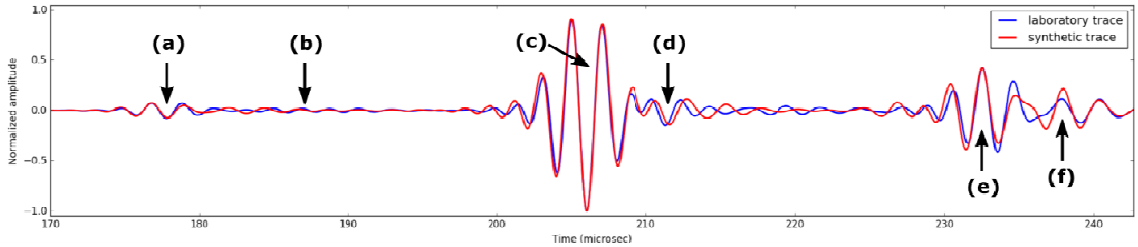

Figure 5 *Comparison of laboratory trace with synthetic result for trace 371. Annotated events are discussed in the text.*

Discussion and conclusions

We have reproduced real laboratory measurements with high precision, using FEM with a structural mesh. Comparison of laboratory data and synthetic results shows a good fit. To reach this good fit one has to account for 3D effects and viscoelasticity, as well as accurately implementing the characteristics of the real transducers used for the laboratory measurements. Furthermore, using a structural mesh, one has to optimize for the number of elements to reduce the computational cost as much as possible. We have showcased some small discrepancies between the real and synthetic data, which can for instance be related to noise in the laboratory data or not accurate radiation pattern implementation of the transducer. Checking the effect of all these issues and improving them will be part of our future work, as well as optimizing further the meshing process and comparing the results with other numerical methods (e.g. FDM). Last but not least, doing a quantitative misfit analysis for phase and envelop misfits and comparing laboratory and synthetic results for multi-offset configuration will also be performed in the future.

Acknowledgements

This project has received funding from the European Union's Horizon 2020 research and innovation program under the Marie Skłodowska-Curie grant agreement No 641943. We also thank CNRS for financial support through PICS BENCHIE project.

References

Bretaudeau, F., Leparoux, D., Durand, O. and Abraham, O. [2011] Small-scale modeling of onshore seismic experiment: A tool to validate numerical modeling and seismic imaging methods. *Geophysics*, **76**(5):T101-T112.

Chen, G. [1996] Comparison of 2-D numerical viscoelastic waveform modeling with ultrasonic physical modeling. *Geophysics*, **61**(3):862-871.

Evans, J.F. [1959] Seismic model experiments with shear waves. Geophysics, **24**(1):40-48.

Favretto-Cristini, N., Tantsereva, A., Cristini, P., Ursin, B., Komatitsch, D. and Aizenberg, A.M. [2014] Numerical modeling of zero-offset laboratory data in a strong topographic environment: results for a spectral-element method and a discretized Kirchhoff integral method. *Earthquake Science*, **27**(4):391-399.

French, W.S. [1974] Two-dimensional and three-dimensional migration of model-experiment reflection profiles. *Geophysics*, **39**(3):265-277.

Komatisch, D. and Vilotte, J.P. [1998] The spectral-element method: an efficient tool to simulate the seismic response of 2D and 3D geological structures. *Bulletin of the Seismological Society of America*, **88**(2):368-392.

Sandia National Laboratories [2016] Cubit 15.2. Albuquerque, NM, USA.

Tantsereva, A., Ursin, B., Favretto-Cristini, N., Cristini, P. and Aizenberg, A.M. [2014] Numerical modeling of 3D zero-offset laboratory data by a discretized Kirchhoff integral method. *Geophysics*, **79**(2):T77-T90. + Errata: *Geophysics*, **79**(5):Y3-Y4

Tromp, J., Komatitsch, D. and Liu Q. [2008] Spectral-element and adjoint methods in seismology. *Communications in Computational Physics*, **3**(1):1-32.